



The effect of contactless support parameters on the mechanical properties of laser powder bed fusion produced overhang parts

Orhan Gülcan¹ · Kadir Günaydın¹ · Alican Çelik¹ · Evren Yasa²

Received: 28 June 2022 / Accepted: 11 September 2022 / Published online: 13 September 2022
© The Author(s), under exclusive licence to Springer-Verlag London Ltd., part of Springer Nature 2022

Abstract

Support structures are used in especially overhang areas in laser metal additive manufacturing to prevent parts from distortion due to high thermal gradients. Since the support structures are not a part of the final component, extra time and material are needed for manufacturing. Moreover, they need to be removed after the build is completed. In addition to waste of time and material, distortion and/or surface roughness issues at supported surfaces may be observed during support removal. As a solution, contactless supports with no direct contact between the support and the part are studied in the present work. Contactless support gap, thickness of each contactless support pieces, and the spacing between two contactless support pieces were used as design variables, and dimensional variations, microhardness through thickness, microstructural changes of bottom surfaces, and surface roughness of overhang features were selected as performance outputs. A full set of design of experiments were manufactured by laser powder bed fusion process using Inconel 718 material. It was observed that all three geometrical parameters had influence on the performance outputs.

Keywords Laser powder bed fusion · Contactless support · Dimensional variation · Surface roughness · Microhardness

1 Introduction

Today, additive manufacturing (AM) technologies are used in a wide range of different industries to produce very complex parts with acceptable mechanical properties, tolerances, and costs which are very difficult or sometimes impossible to produce with conventional manufacturing processes [1]. Laser powder bed fusion (LPBF) is one of the metal AM technologies where powder is laid on a platform layer by layer with a recoater blade and the laser energy is used to melt the powder according to the machine-specific tool path

based on a 3D computer-aided design file sliced in a virtual environment [2].

As well as other powder bed fusion processes, LPBF is a thermal process, and therefore, some problems due to large thermal residual stresses like warping, sagging, or shrinkage may occur after manufacturing affecting the dimensional accuracy and mechanical performance of the final part. To reduce this effect, during pre-processing, support structures are added to especially overhang areas inclined with respect to the build plate with an angle less than 45° [3, 4]. These support structures need to prevent the part from distortion due to high thermal gradients, and they also act as an anchorage to the base plate [5]. Yet, support structures are not a part of the final component, and they need to be removed after the build process is completed although being a key factor for manufacturability. Therefore, an additive design engineer needs to consider not only the production time, cost, and success but also the removability of supports from the built geometry during pre-processing [6]. Also, removing support structures after the build process may cause some additional problems such as undesired distortions and/or surface roughness issues at mating areas [7].

Different studies have been performed to eliminate the need of support structures or to investigate design rules for

✉ Orhan Gülcan
orhan.gulcan@ge.com

Kadir Günaydın
kadir.gunaydin@ge.com

Alican Çelik
alican.celik@ge.com

Evren Yasa
eyasa@ogu.edu.tr

¹ General Electric Aviation, Gebze, Kocaeli 41400, Turkey

² Mechanical Engineering Department, Eskişehir Osman Gazi University, Eskişehir, Turkey

manufacturing overhang parts without support structures. Ameen et al. investigated the producibility of different types of overhang geometries without support and stated that convex overhangs up to a 7-mm radius, concave overhangs up to an 8-mm radius, slope overhangs up to 50° edge, and bridge overhangs up to 5 mm in length can be built without support structures [8].

In AM, support structures dissipate heat during process and help to reduce distortions and dimensional deviations due to residual stresses. Since different support geometries have different thermal conductivities, their effects on distortion and deviation of the produced parts are also different [9]. Different support types were used in the literature to better estimate these effects: block support, point support, web support, contour support, line support [10], Y supports, inverted Y supports, pin supports etc. [11]. Lindecke et al. stated that for better dimensional accuracy, the support structure needs to be connected to the part, and this connectivity length (teeth length) for teeth supports needs to be minimum 0.1 mm [12]. The importance of the teeth height on warpage of LPBF parts with tooth support was studied by Calignano [13]. It was revealed that the teeth height has the biggest impact on S/N (signal to noise) ratios for both AlSi10Mg and Ti6Al4V samples [13]. Poyraz et al. investigated the effect of different block supports with different hatch distances and fragmentation intervals and tooth supports with different top lengths (length of connection between support and the part) and Z-offsets (offset between top of tooth support and mating surface of parts) on the deformation of bridge-like structures. They concluded that for block supports, increasing the hatch distance increased the distortion on the part, and hatching parameters had higher influence on support structure than tooth parameters [14]. Umer et al. investigated the effect of support structure type on the deformation of Ti6Al4V parts produced by electron beam powder bed fusion (EPBF), another type of PBF processes. They used column and Y-shape supports and stated that there was a nearly 22% deviations between experimental and simulation results. The authors attributed this deviation to the assumption that there was no deformation in lateral direction and to deviations in material properties and lastly to deformations in base plate before printing process [15]. Ameen et al. used tooth supports in overhang parts produced by EPBF and stated that supports with 3 mm tooth height, 0.05 mm tooth top length, and 3.5 mm tooth base interval reduced the support removal time significantly [16]. Hussein et al. used gyroid and diamond lattice support structures for overhang parts and stated that when the cell size increased, the manufacturability of parts decreased [17]. Cao et al. investigated the removability of cone and block support structures in LPBF manufactured AISI 316L stainless steel parts with milling and stated that block support is more favorable than cone support since the block

supports are strong enough to prevent distortion and the milling forces required to remove the block support is lower [7]. Leary et al. investigated the effect of support height and support spacing on contact strength between support and built part under normal and peel loading conditions and concluded that contact strength is not affected much by support spacing with a given support height [4]. Järvinen et al. investigated removability and surface quality of laser LPBF parts with web and tube supports and stated that web supports showed better behavior [6]. Apart from the support structure types, some researchers focused on changing the build orientation or process parameters to reduce the need for support structure. Since the support structure is mostly needed in overhang areas, changing the build orientation of part with respect to build plate may significantly reduce the need for support structure [18, 19]. However, for complex geometries, this remedy may create other regions in need of support. The scanning strategy of the overhang features affects deformation behavior in LPBF. In one of the studies, it was revealed that parts scanned in transverse direction (y direction) showed less deformation than parts scanned in longitudinal direction (x direction) due to less residual stress observed on overhangs [20]. However, it is not correct to generalize this result because the effect of the scan direction shall be evaluated together with the part geometry.

As stated in most of the scientific papers, 45° angle is taken as the threshold value for the support structure need in AM although newer studies can further reduce this angle. Different studies have been performed to redesign and optimize the parts for making overhang surfaces as self-supporting. Allaire et al. presented different mathematical models and algorithms to obtain optimal support structure designs [21]. Das et al. investigated the optimum build orientation which minimizes support structure volume and contact area between

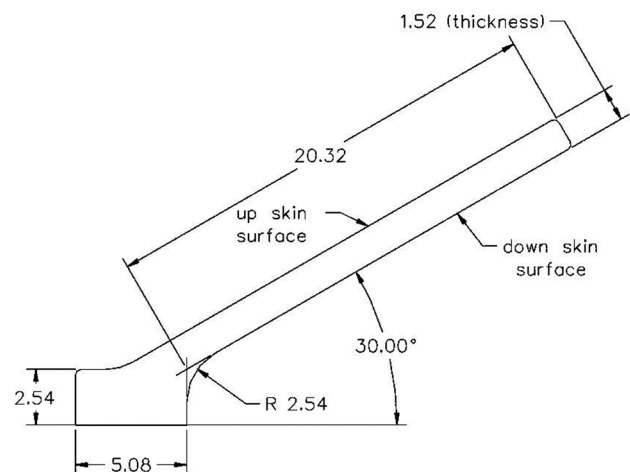


Fig. 1 Dimensions of overhang specimen (all dimensions are in mm; width, 25.4 mm)

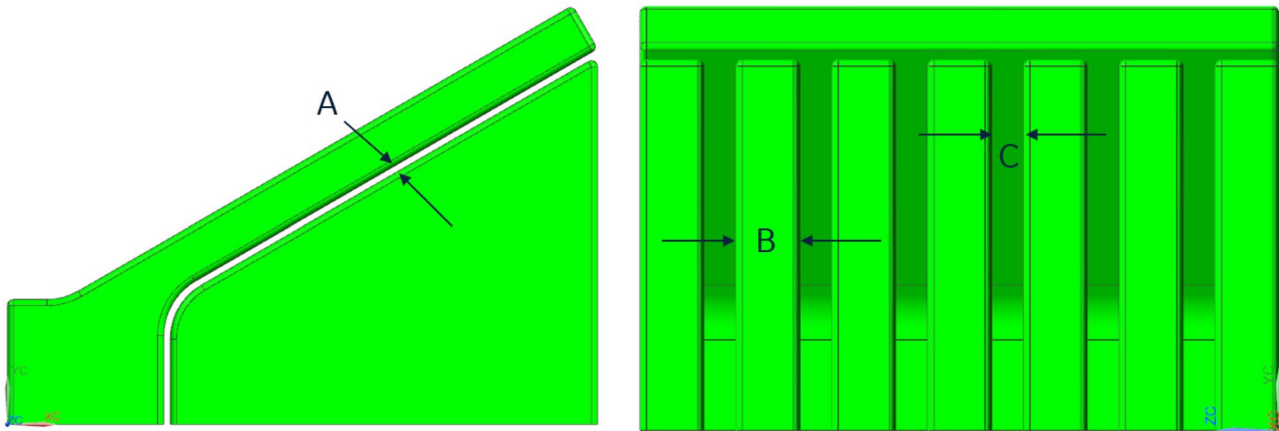


Fig. 2 Design variables: support gap (A), thickness of each support pieces (B), and spacing between two support pieces (C)

the support and the part and maximizes the percentage of removable support structure material while satisfying flatness, cylindricity, perpendicularity, and parallelism tolerances [22]. Kuo and Cheng used a logistic aggregate function for self-supporting design methodology based on topology optimization by using overhang angle as a manufacturing constraint [3]. Pellens et al. used topology optimization on support structures by using maximum allowable vertical displacement in each layer to avoid recoater collision problems [23]. Allaire et al. used shape and topology optimization of support structures by applying pseudo-gravity loads and equivalent thermal loads on overhanging surfaces and by using penalization on unnecessary contact between the part and the support [24]. Zhou et al. used a density-based topology optimization method for designing easy-to-remove self-supporting support structure which bears the weight of additive manufactured part [25]. Optimization of the support geometries in terms of weight, ease of removal, and heat diffusivity was studied by Zhang et al. They generated biomimetic support structures by performing genetic algorithm [26]. Zhou et al. used gradient-based topology optimization method to design thermally conductive support structures [27]. Some authors used topology optimization to obtain optimized support geometries where machine tools are accessible from a prescribed tool approach direction [28, 29].

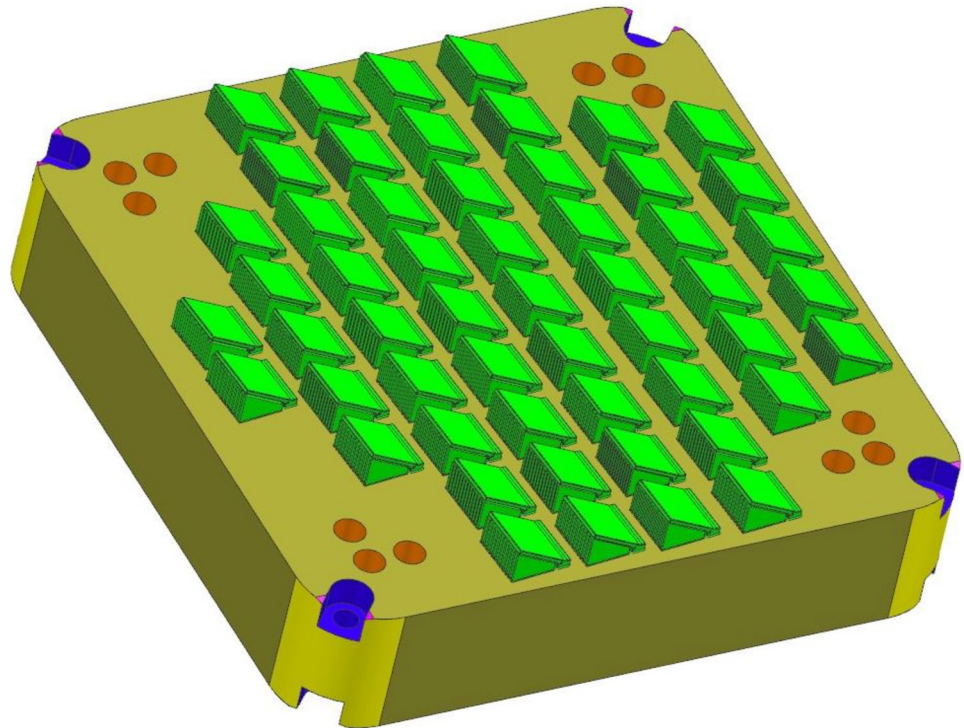
In some scientific studies, support structures are categorized as active and passive support structures where there is no contact between the support and the part and the support is “floating” in the powder in passive support structures. On the other hand, there is a direct connection between support surface and mating part’s surface in active support structures [30]. In the present study, these “passive support structures” are called contactless supports. Since the removability of support structures after manufacturing means extra time and cost, contactless supports where there is no direct connection between the part and support help to reduce the

efforts spent on removing these structures. In literature, it was stated that contactless supports act as heat sink which improves heat transfer efficiency, reduces the thermal residual stresses [31], improves mechanical properties, and evolves the microstructures of the part [32]. In contactless

Table 1 Design of experiment (all dimensions are in mm)

Experiment No	A	B	C
1	0.23	0.76	0.51
2	0.23	0.76	0.76
3	0.23	0.76	1.02
4	0.23	1.02	0.51
5	0.23	1.02	0.76
6	0.23	1.02	1.02
7	0.23	1.27	0.51
8	0.23	1.27	0.76
9	0.23	1.27	1.02
10	0.31	0.76	0.51
11	0.31	0.76	0.76
12	0.31	0.76	1.02
13	0.31	1.02	0.51
14	0.31	1.02	0.76
15	0.31	1.02	1.02
16	0.31	1.27	0.51
17	0.31	1.27	0.76
18	0.31	1.27	1.02
19	0.38	0.76	0.51
20	0.38	0.76	0.76
21	0.38	0.76	1.02
22	0.38	1.02	0.51
23	0.38	1.02	0.76
24	0.38	1.02	1.02
25	0.38	1.27	0.51
26	0.38	1.27	0.76
27	0.38	1.27	1.02

Fig. 3 Specimen layout on build plate



supports, the gap between the support and part affects the part distortion. When smaller gaps are used, the part distortion is reduced. However, if small gaps are used and if the melt pool is deeper than the selected gap, there is a possibility of the loose powder between the support and the part to be melted/sintered so that the support is solidified together with top layers of the part [33]. Cooper et al. investigated the feasibility of using contactless supports (in their study, they called it heat support) in different overhang geometries produced by EPBF. They used 0.49 mm, 0.63 mm, and 0.77 mm as contactless support gaps and stated that overhang distortions and effectiveness of contactless supports depend on the gap and thickness values [34]. Zhang et al. investigated the effectiveness of contactless supports in LPBF and used 0.3, 0.45, and 0.75 mm gaps between the support and the overhang surface and stated that the minimum distortion was observed at the smallest gap [35]. Cheng et al. stated that 3 mm or even 0.8 mm thick contactless supports with 0.21 mm gap successfully reduced the deformation on overhang parts produced by EPBF when compared with no support design [36, 37].

As evident from this short literature survey, most of the studies carried out with contactless supports are focused on the EPBF process investigating different design parameters.

To reduce the total cost and time of LPBF parts, contactless supports seem to be a very good alternative to conventional support structures. As observed from the literature review, very few numbers of studies have focused on the effect of using contactless supports on distortion and dimensional deviations of overhang areas for LPBF. In these studies, contactless support gaps were used as design variables. However, support structures can be one piece under overhang regions or many pieces to reduce the amount of powder to be used. When more than one piece of support structure is used, the distance between these pieces and their inclination with respect to build plate is very important in terms of columnar pore formation and mechanical properties of the final part [38]. To the best of the authors' knowledge, no study has focused on the effect of contactless support parameters (gap, thickness, and spacing) on dimensional variations, microhardness, microstructural changes, and surface roughness of overhang features. To fill this gap, this study investigated contactless support gap, thickness, and spacing effects on the aforementioned performance outputs. The rest of the paper is organized as follows: Sect. 2 details the specimen and support design, design of experiment, manufacturing, and measurements. In Sect. 3, experimental design is presented and discussed in detailed in terms of average thickness deviation,

Table 2 Chemical composition of Inconel 718 wt%

Element	Ni	Cr	Nb	Mo	Ti	Mn	Si	Al	Fe
wt %	53.00	18.50	5.00	3.00	0.66	3.00	0.35	0.35	Balance

Table 3 Processing parameters [39]

	Laser power (W)	Laser scan speed (mm/s)	Laser spot size (μm)
Skin	160	800	80
Core	160	680	53

surface roughness of overhang surfaces, and microhardness through the thickness of the specimens.

2 Materials and methods

The overhang specimens with an inclination angle of 30° with respect to build plate were modeled using Siemens NX 12 software (Siemens AG, Germany). The geometry with its dimensions is shown in Fig. 1. Since 45° is the threshold value for an overhang surface below which support structures are needed [3, 4], 30° inclination was used for the specimen in this study. LPBF process is capable of producing parts with a wall thickness of greater than 1 mm (at most 0.5–0.6 mm). Therefore, in this study, thin wall specimens with 1.52 mm (0.06 inch) wall thicknesses were used to prevent build failure. To make surface roughness and dimensional variation measurements effectively, the measurement area was designed to be nearly 20×25 mm (0.8×1.0 inch). The contactless supports having some amount of gap with the overhang specimen were used during production. The gap between the contactless support and the overhang part, the thickness of each contactless support pieces, and the spacing between two contactless support pieces were used

as design variables as shown in Fig. 2. Support structure was added only under downskin surface of the specimen since only this surface has an inclination less than 45° with respect to build plate. A full set of design of experiments was used in this study with three factors at three levels. Table 1 shows the related data for the total 27 experiments. Initial trials have shown that overhang specimens can be produced without any failure when the contactless support gap is between 0.23 mm (0.009 inch) and 0.38 mm (0.015 inch). Below 0.23 mm support gap, it was observed that support structure was fused to the specimen. On the other hand, above 0.38 mm support gap, build failures were observed in some of the specimens. Therefore, 0.23 mm, 0.31 mm, and 0.38 mm support gaps were used in the present study. The thickness of each segment was selected as 0.76 mm (0.03 inch), 1.02 mm (0.04 inch), and 1.27 mm (0.05 inch) to prevent build failure due to thin wall production and to ease the removal of supports from build plate. The spacing between two support segments was selected as much as lower (0.51 mm (0.02 inch), 0.76 mm (0.03 inch), 1.02 mm (0.04 inch)) to prevent melt pool sagging during production due to gravity.

The specimens were located on the build plate as shown in Fig. 3 where the powder recoater direction is from right to left. For each configuration of 3 factors, three specimens, in other words repetitions, and a total of 81 specimens were produced in two builds.

The specimens were manufactured using a Concept Laser M2 LPBF machine (Concept Laser GmbH, GE Additive, Germany) from Inconel 718 material. DMLM manufacturing was performed under nitrogen gas environment, and 50- μm layer thickness was used. The chemical composition

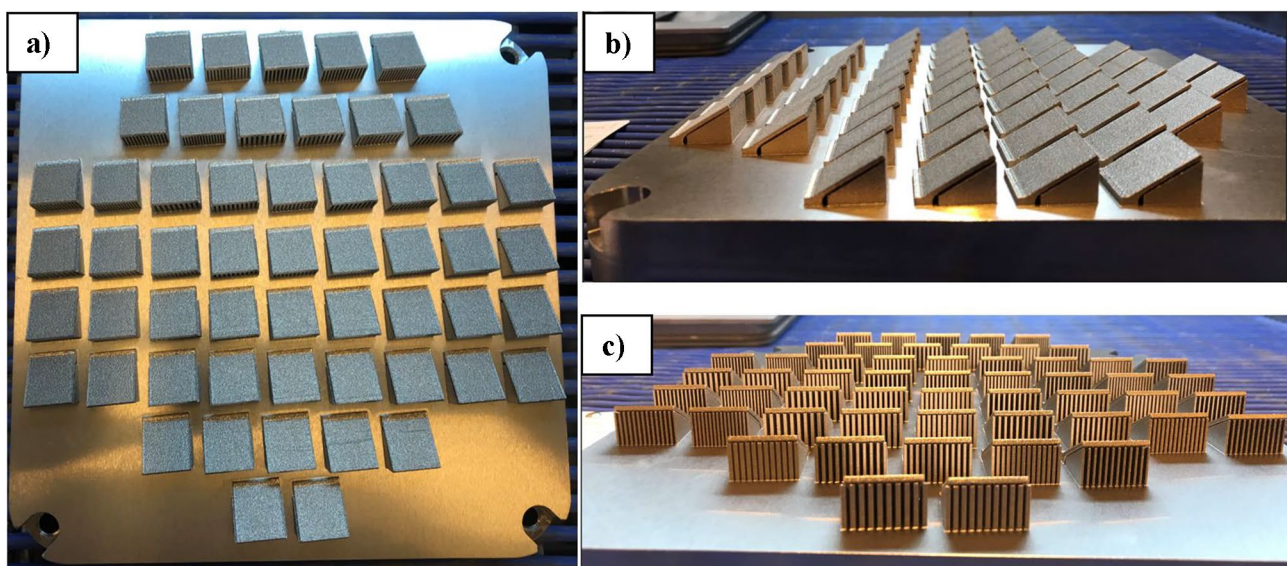


Fig. 4 Produced specimens after powder removal: **a** top view, **b** side view, **c** front view

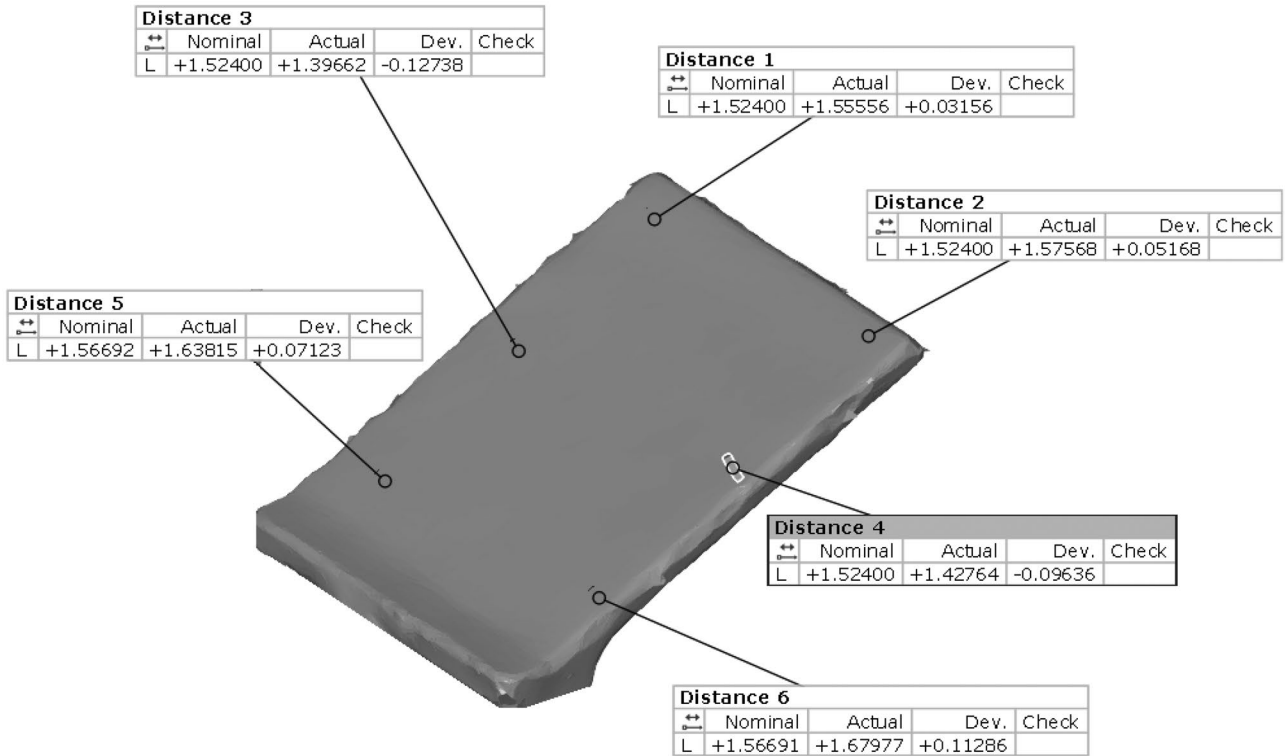


Fig. 5 Surface deviation measurements from 6 locations

of the Inconel 718 material used in production is shown in Table 2, and the standard vendor process parameters were used during manufacturing as presented in Table 3.

After manufacturing, powder evacuation process was performed on Solukon SFM-AT800 system (Solukon Maschinenbau GmbH, Augsburg, Germany). GF AgieCharmilles wire electrical discharge machine (AgieCharmilles Ltd., Switzerland) with wire thickness of 0.3 mm and an average cutting

speed of 5 mm/min was used for removing specimens from the build plate.

The manufactured specimens were scanned with ATOS ScanBox 4105 blue light device (Carl Zeiss GOM Metrology GmbH, Braunschweig, Germany). GOM Inspect software (Carl Zeiss GOM Metrology GmbH, Braunschweig, Germany) was used to evaluate the scan results and investigate the dimensional variations of the produced

Fig. 6 The effect of support thickness and spacing on average thickness deviation for 0.23 mm support gap

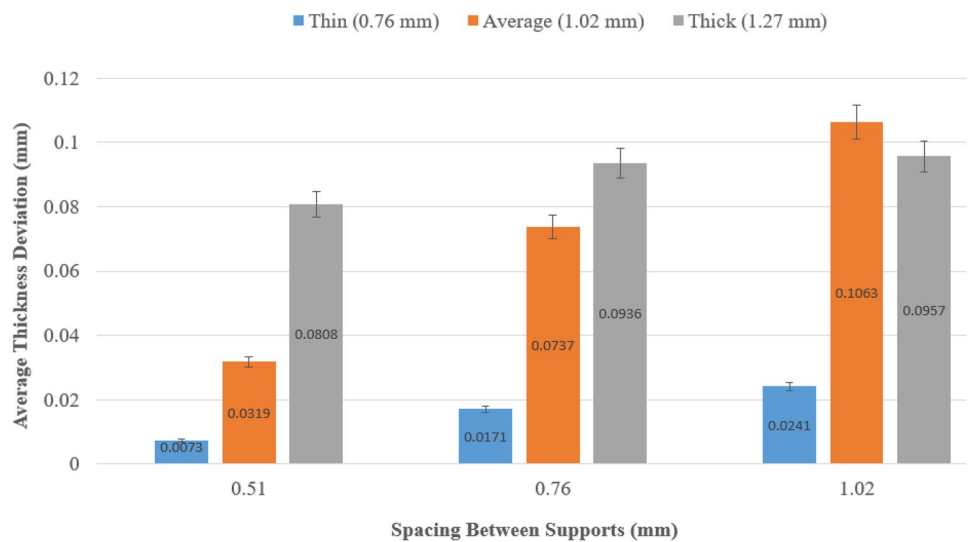
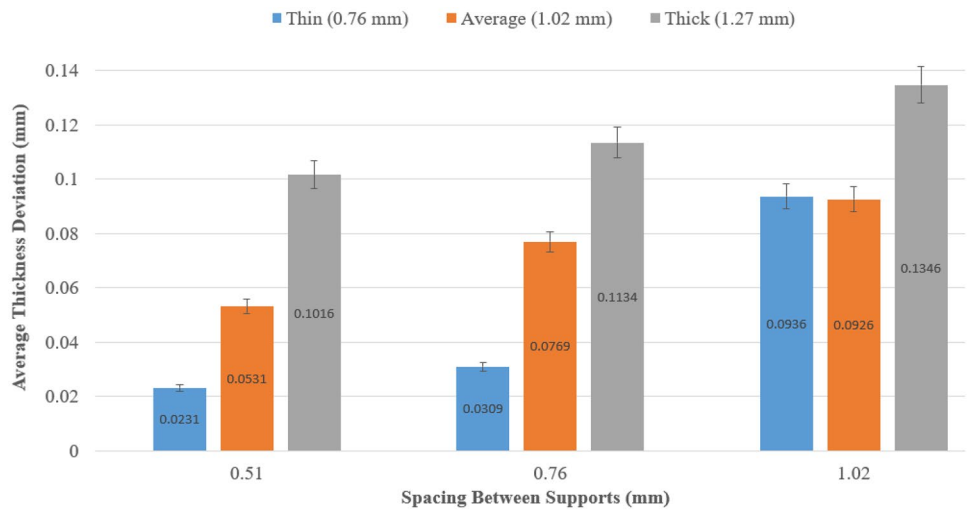


Fig. 7 The effect of support thickness and spacing on average thickness deviation for 0.31 mm support gap



specimens. For surface roughness measurements, Alicona InfiniteFocus G5 (Alicona Imaging GmbH, Graz, Austria) was used based on focus variation technique. $\times 10$ magnification, polarized coaxial illumination, 6 μm lateral resolution, and 900 nm vertical resolution were used during surface roughness (S_a) measurements. For metallographic studies and microhardness measurements, the overhang specimens were cut from their middle locations with Struers Secotom cutter, mounted in Struers CitoPress mounting machine, and finally polished with Struers Tegramin (Struers LLC, Ohia, US). Nikon Eclipse MA200 optical microscope (Nikon corp., Tokyo, Japan) and Zeiss Merlin FE-SEM scanning electron microscope (Carl Zeiss AG, Jena, Germany) were used for metallographic studies. The hardness measurements were conducted by Emco-Test DuraScan-70 type microhardness tester equipment (EMCO-TEST Prüfmaschinen GmbH, Kuchl, Austria) at Vickers hardness scale 0.3 (HV 0.3, 2.942 N). The three microhardness measurements were conducted through the

thickness of the specimens from the upper to the lower surface (at the near upper edge, at the middle, and at the near lower edge). For all measurements, three specimens for each experiment set were measured, and the average values were used in the evaluations.

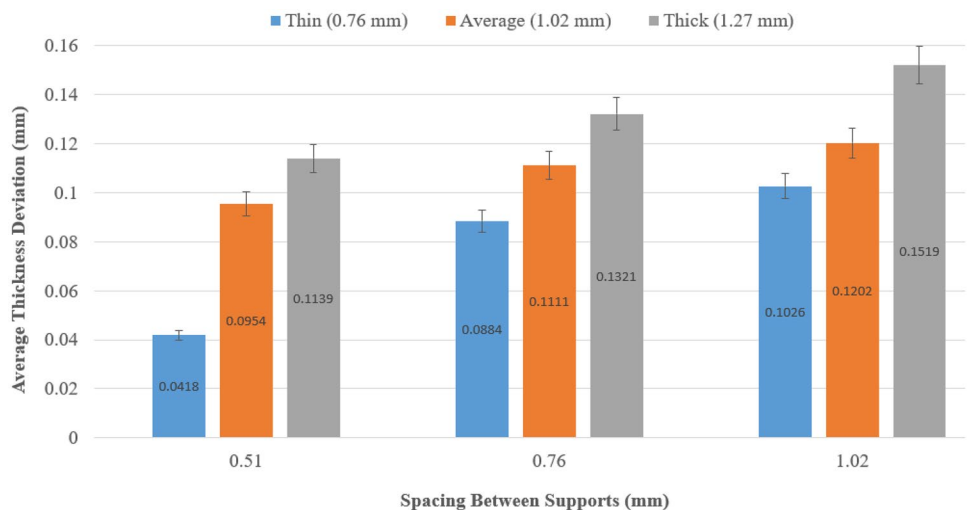
3 Results and discussions

All specimens were successfully produced without any production problem as depicted in Fig. 4. All contactless supports and specimens were removed from the build plate, and it was observed that there is no partial or full fusion of any support with the specimens.

3.1 Dimensional deviation results

For each specimen, surface deviations were measured from 6 locations as shown in Fig. 5. The average thickness deviations

Fig. 8 The effect of support thickness and spacing on average thickness deviation for 0.38 mm support gap



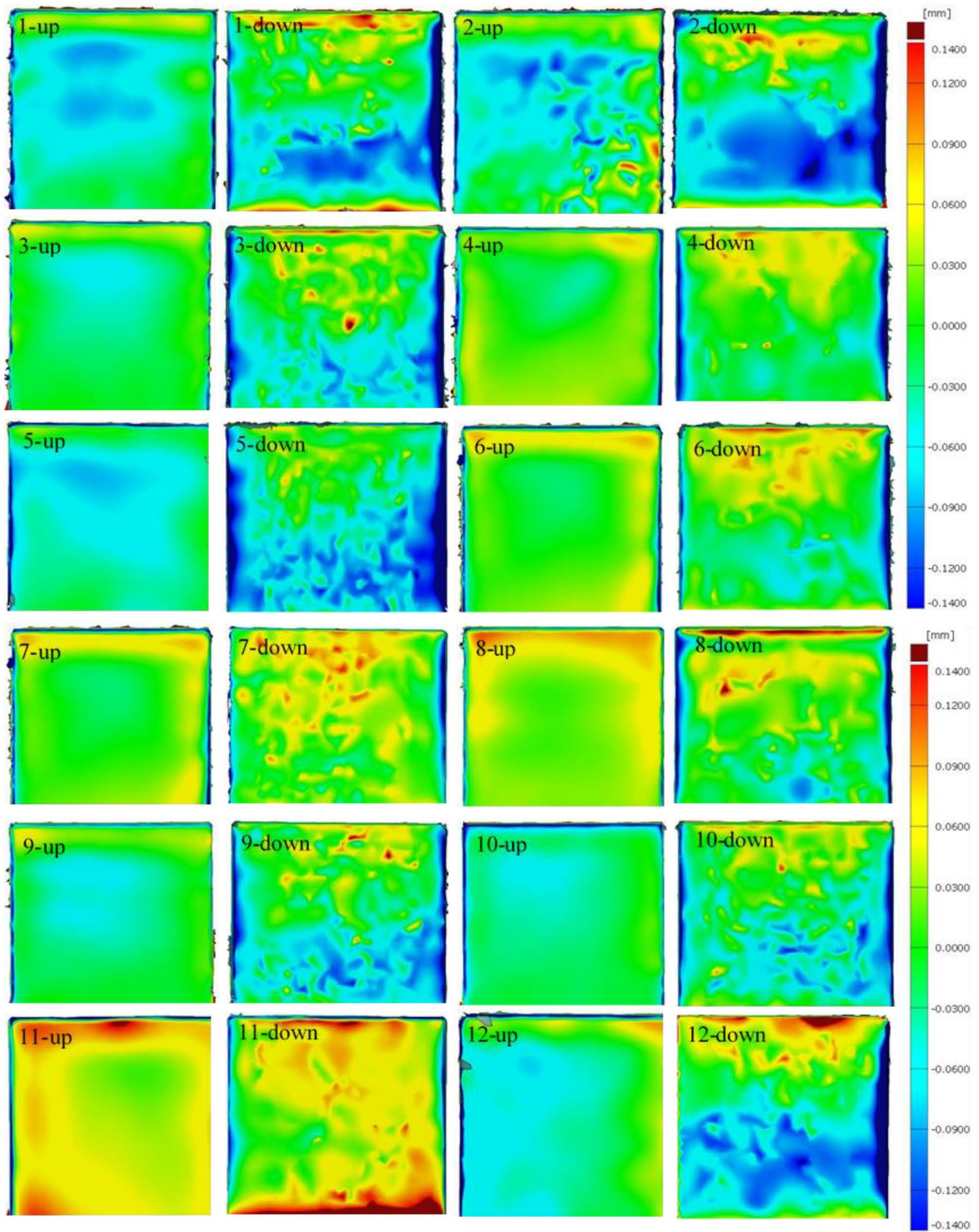


Fig. 9 The deviations of up- and downskin surfaces for all specimens

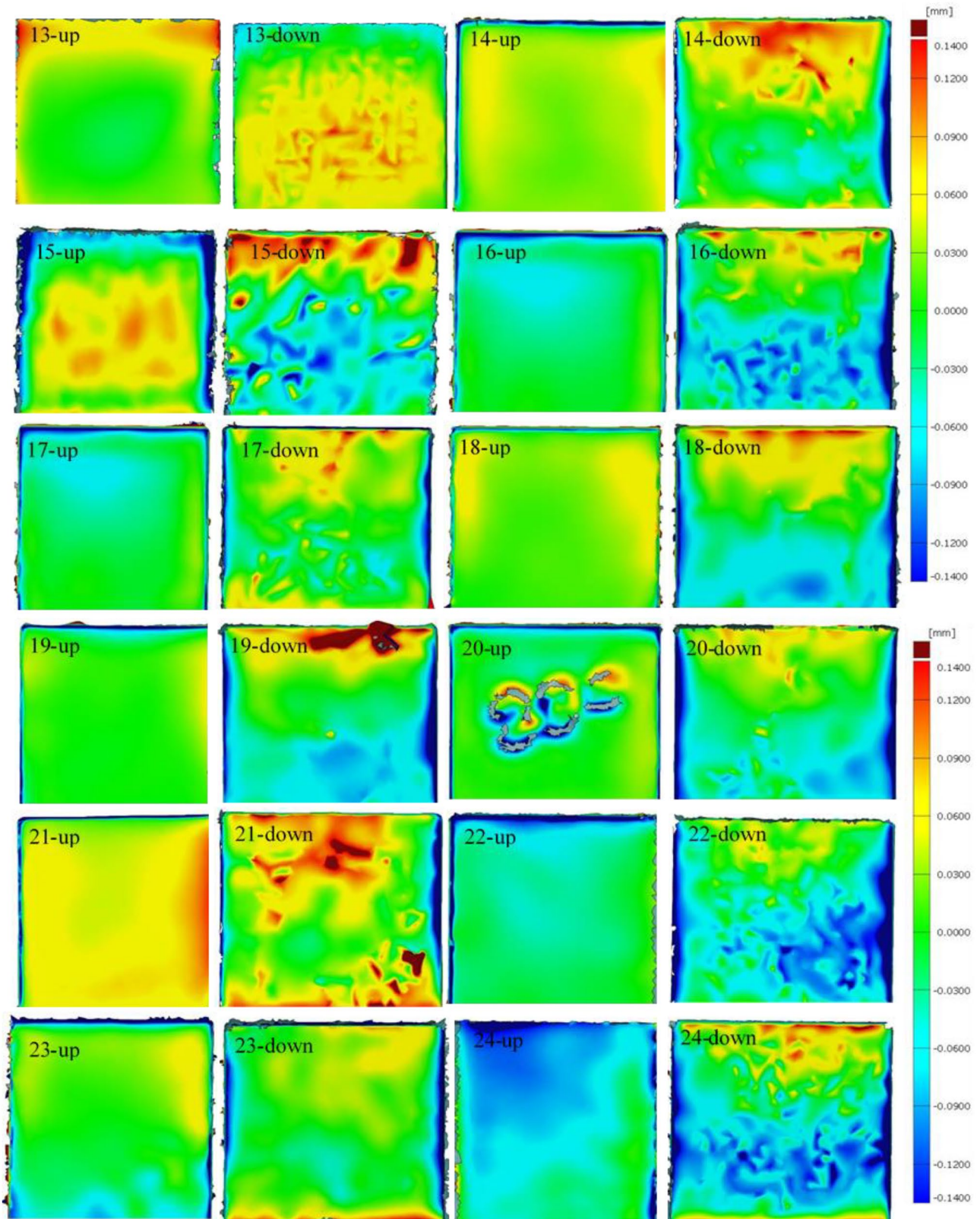


Fig. 9 (continued)

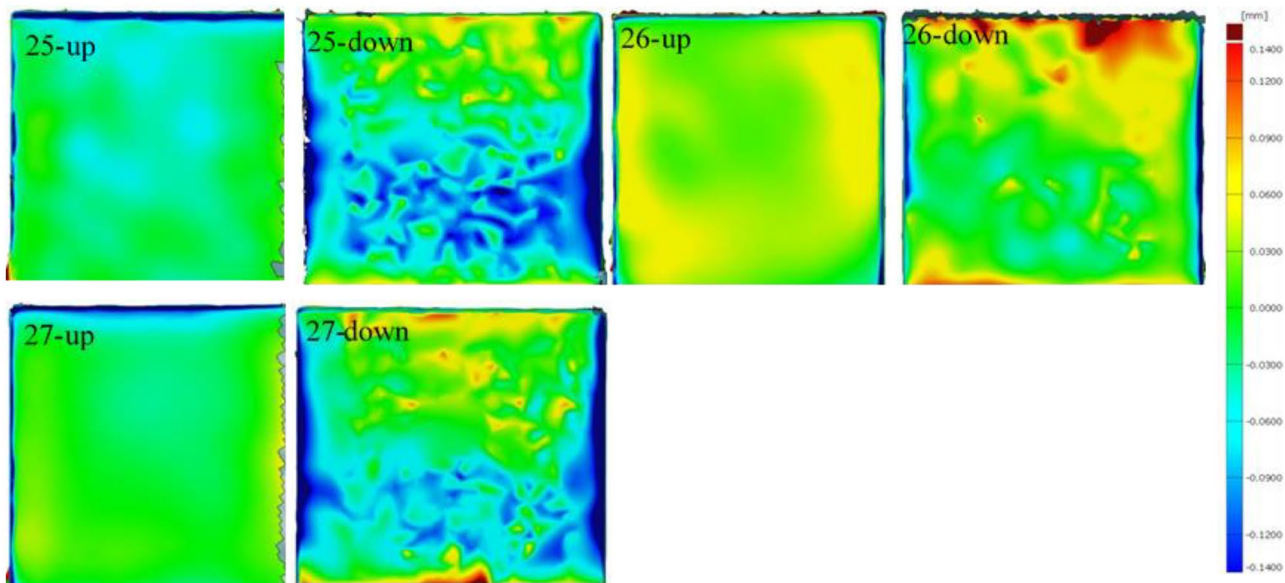


Fig. 9 (continued)

are shown in Figs. 6, 7 and 8 in terms of support thickness and support spacing for three different support gap values. Deviations of up and downskin faces of each specimen are shown in Fig. 9.

It is clear from Figs. 6, 7 and 8 that average thickness deviation increases with an increase in support thickness, support spacing, or support gap. This can be attributed to the fact that when contactless support gaps are increased, the powder between the support and the specimen can't provide enough heat dissipation, and melt pools freestanding on downskin surfaces penetrate towards the powder bed, causing more non-fully melted powders sticking to the melt pool and finally increasing the thickness [40]. The

melt pool sagging and non-fully melted powder adhesion phenomena were also observed in different studies [41–43]. The minimum average thickness deviation (0.0073 mm) was observed when 0.23 mm support gap, 0.76 mm support thickness, and 0.51 mm support spacing were used. On the other hand, the maximum average thickness deviation (0.1519 mm) was observed when 0.38 mm support gap, 1.27 mm support thickness, and 1.02 mm support spacing were used. When spacing between supports increased from 0.51 to 0.76 mm and from 0.76 to 1.02 mm, average thickness deviation for 0.23 mm support gap increased nearly 134% and 41%, respectively, for 0.76 mm support thickness; 131% and 44%, respectively, for 1.02 mm support

Fig. 10 The effect of support thickness and spacing on surface roughness for 0.23 mm support gap

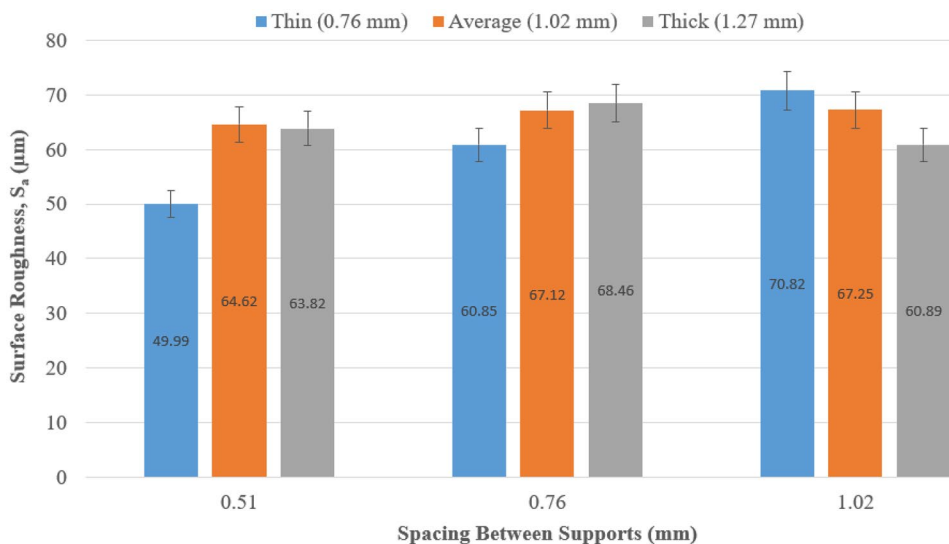
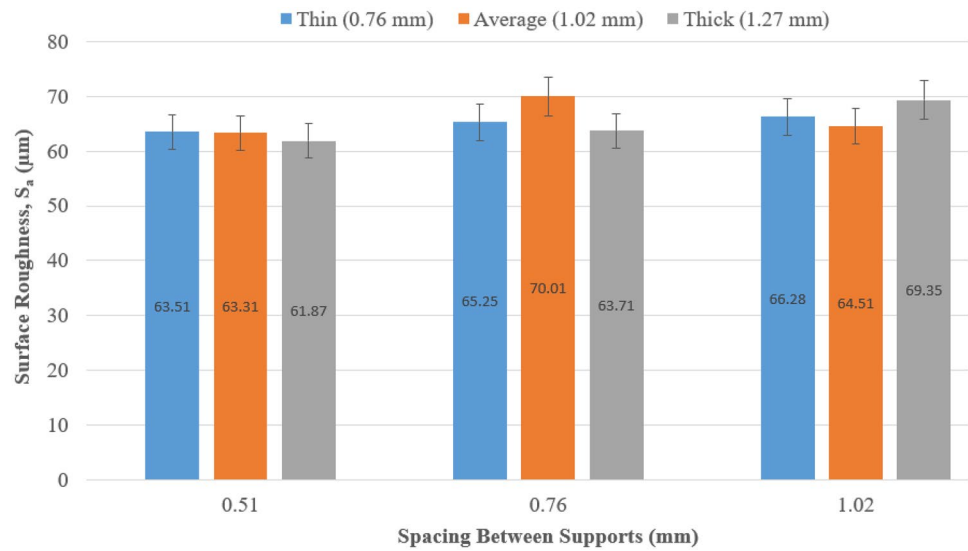


Fig. 11 The effect of support thickness and spacing on surface roughness for 0.31 mm support gap



thickness; and 16% and 2%, respectively, for 1.27 mm support thickness. For 0.31 mm support gap, an increase in average thickness deviation was observed as nearly 8.5% and 203%, respectively, for 0.76 mm support thickness; 45% and 20%, respectively, for 1.02 mm support thickness; and finally, 12% and 19%, respectively, for 1.27 mm support thickness. For 0.38 mm support gap, an increase in average thickness deviation was observed as nearly 111% and 16%, respectively, for 0.76 mm support thickness; 16.5% and 8%, respectively, for 1.02 mm support thickness; and, 16% and 15%, respectively, for 1.27 mm support thickness. It can be concluded that for each of three different support gaps, the percentage of increase in thickness deviation related with an increase in support spacing is higher for thinner supports.

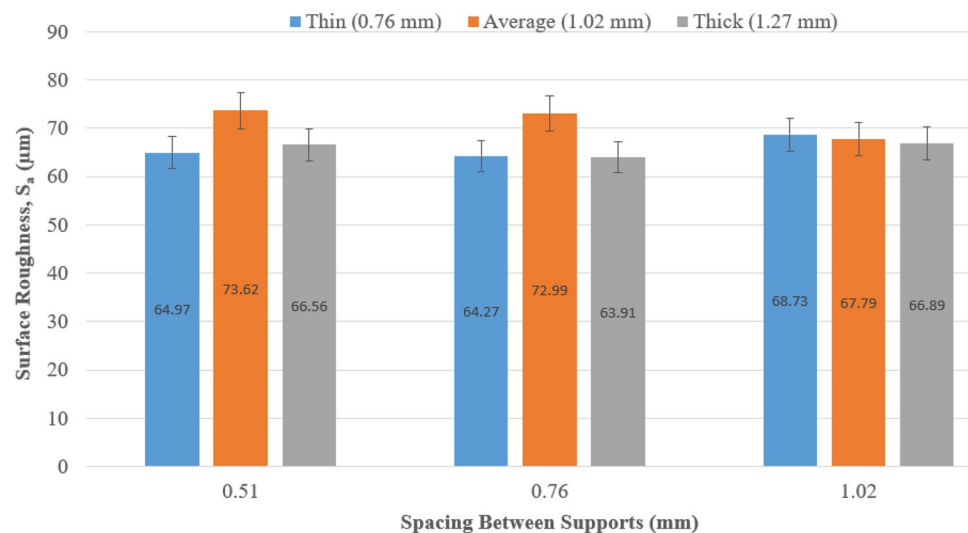
It is clear from Fig. 9 that downskin surfaces have higher deviations than up faces. Smooth deviation was observed on up faces; on the other hand, complicated and different

amounts of deviations were observed on downskin faces from the root to the tip of the specimen. This can be attributed to the fact that downskin surfaces for different specimens were supported by contactless supports of different amounts of support gaps, support spacing, and support thickness resulting in different heat dissipation behaviors. It is also observed that the deviation increases towards the tip of the specimen. Since root of the specimens has a contact with base plate, this hard connection or anchorage results in less deviation; however, towards the specimen tip region, deviation increases since contactless support can't provide enough heat dissipation to these free edges.

3.2 Surface roughness results

Figures 10, 11 and 12 show the effect of support thickness and support spacing on surface roughness for different support

Fig. 12 The effect of support thickness and spacing on surface roughness for 0.38 mm support gap



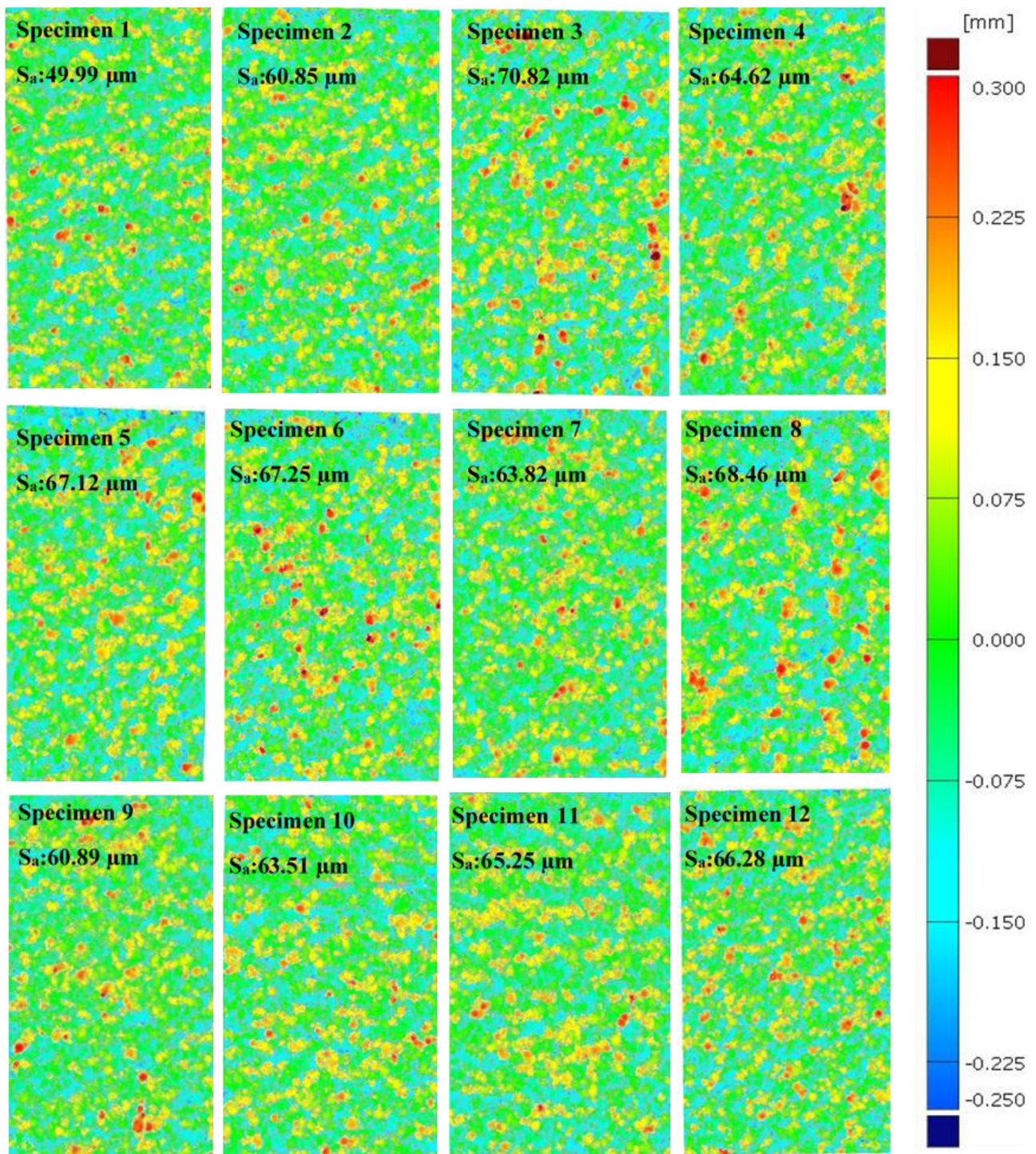


Fig. 13 Surface texture maps for all specimens

gap values. The minimum surface roughness ($49.99 \mu\text{m}$) was observed at 0.23 mm support gap, 0.51 mm support spacing, and 0.76 mm support thickness. On the other hand, the maximum surface roughness ($73.62 \mu\text{m}$) was observed at 0.38 mm support gap, 0.51 mm support spacing, and 1.02 mm support

thickness. It is not always the case, but in general, for fixed support gap and support thicknesses, surface roughness increased with an increase in support spacing.

Figure 13 shows the Alicona measurement results (surface texture maps) for downskin surfaces of all specimens.

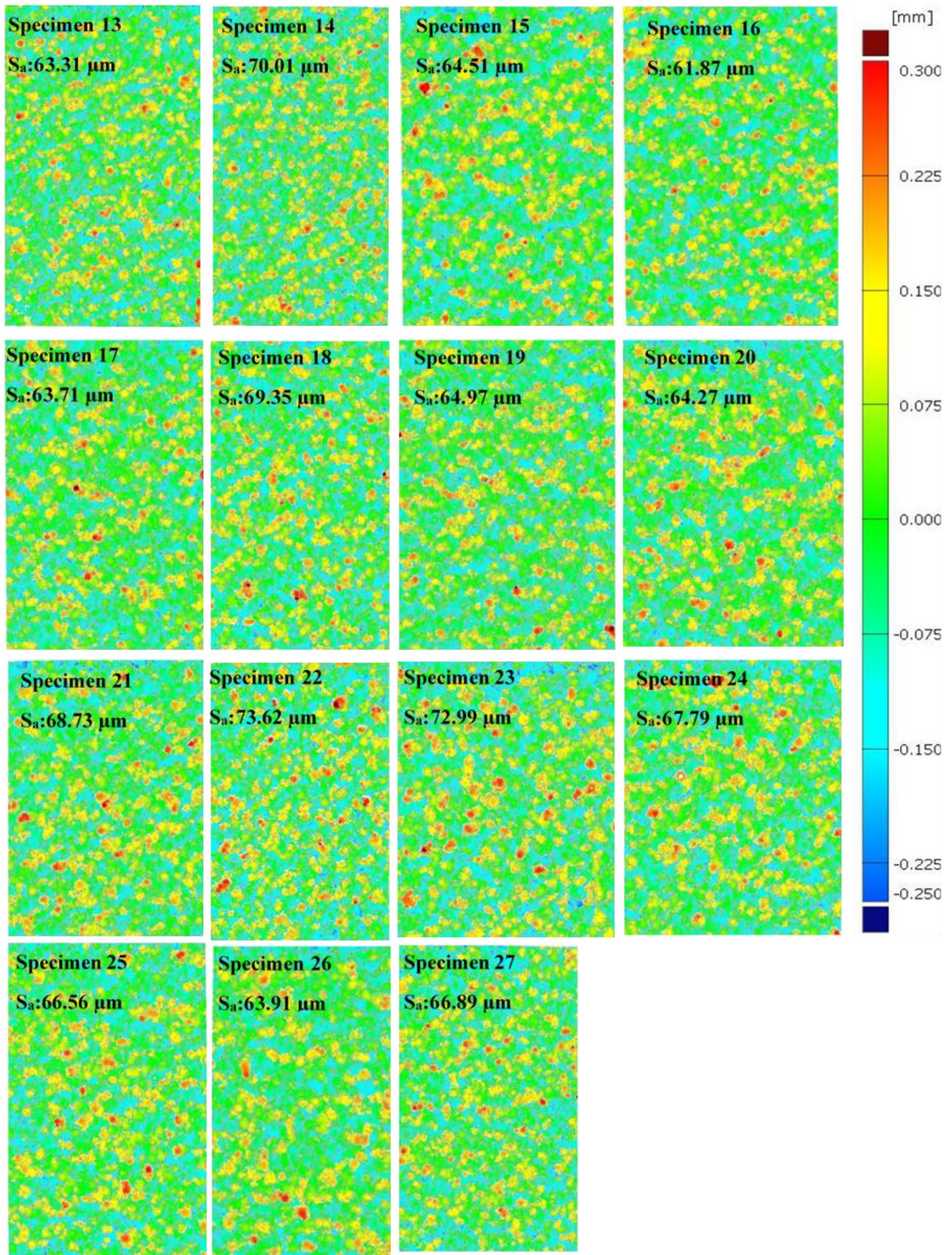
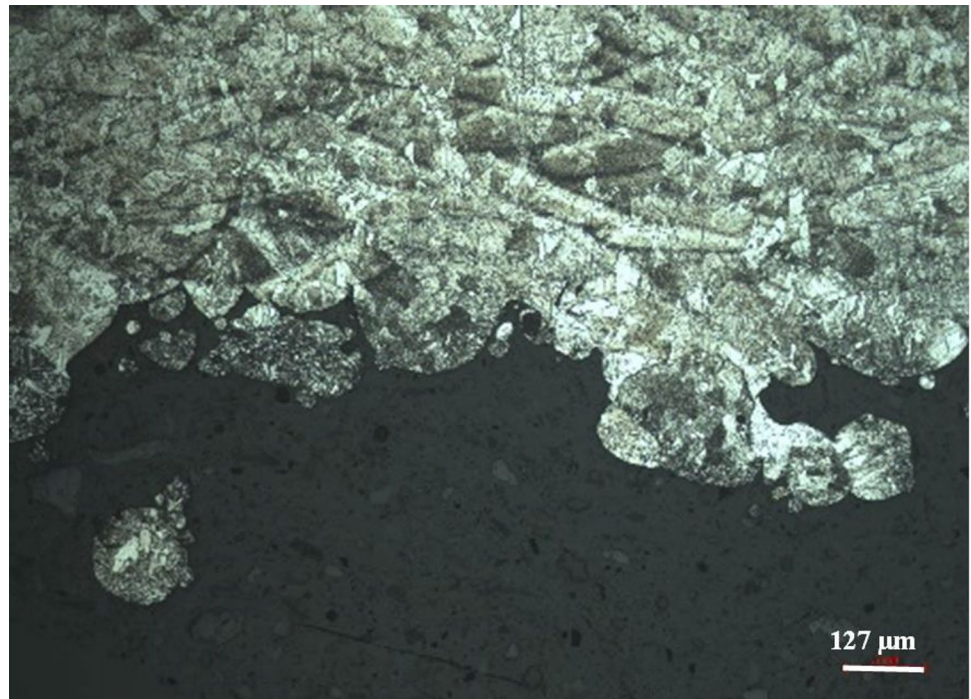


Fig. 13 (continued)

Fig. 14 Optical microscope image of the downskin surface of specimen 8



Surfaces of each specimen consist of valleys and peaks, and deviation of these from mean plane represents the surface roughness. In these maps, valleys are represented as blue and blue-green color, whereas peaks are represented as red, yellow, and yellow-green color. The fraction of valleys and peaks are consistent with the surface roughness values in Figs. 10, 11 and 12. For instance, comparing specimens 1, 2, and 3 shows that the percentage of peaks, meaning the number of red areas, increases from specimen 1 to 2 and 2 to 3, which supports the statement that surface roughness

increased with an increase in support spacing for fixed support gap and support thicknesses.

One of the disadvantages of Alicona measurement is that it heavily depends on the surface profile where there might be some data loss if there is no proper line of sight [44]. Therefore, using optical microscope of the downskin surfaces is a good approach to verify the surface roughness measurements by Alicona. The optical microscope image of downskin surface of specimen 8 was shown in Fig. 14. It is evident from Fig. 14 that there are different surface

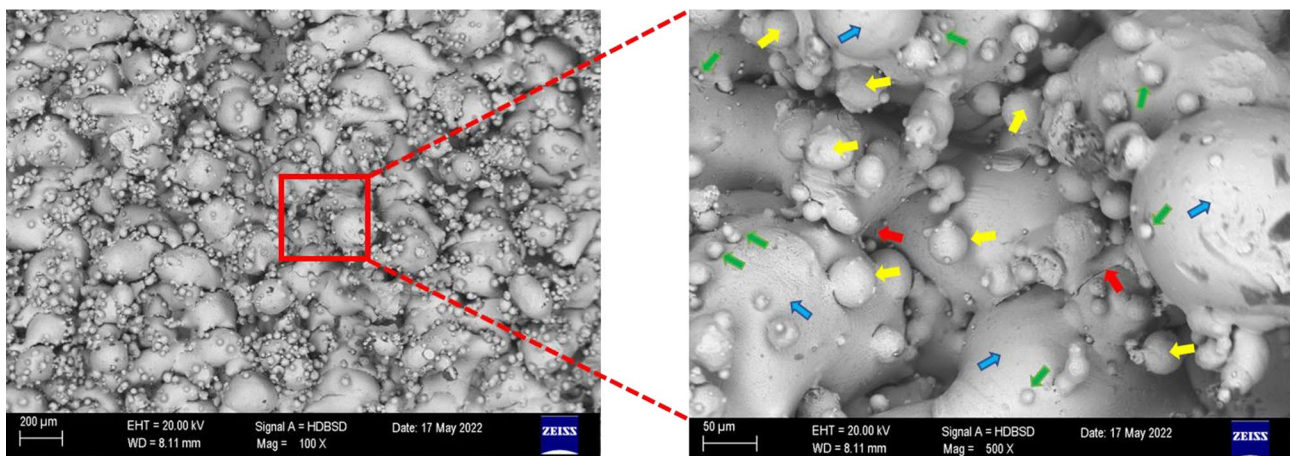
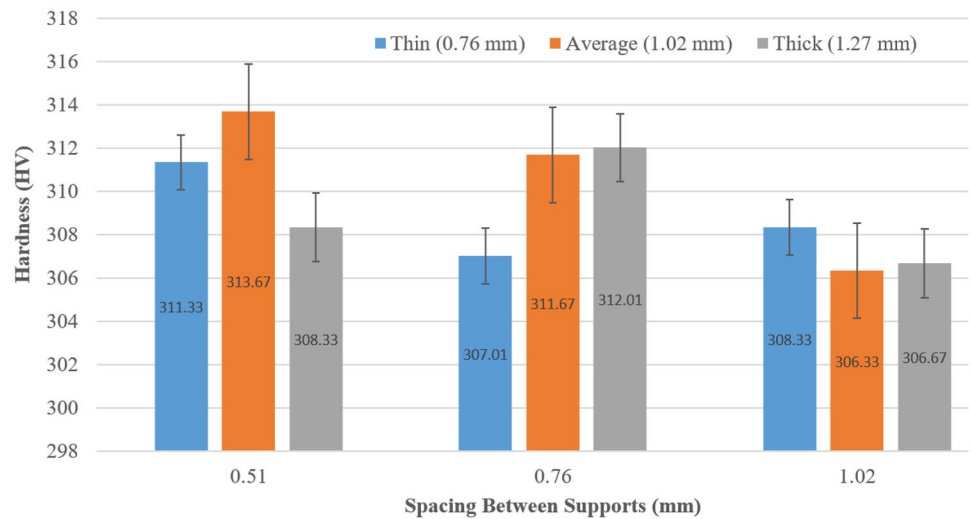


Fig. 15 SEM image of the downskin surface of specimen 2

Fig. 16 The effect of support thickness and spacing on microhardness for 0.23 mm support gap



discontinuities resulting to valleys and peaks with different heights and finally to different surface roughness values. SEM images can reveal these surface discontinuities more clearly. Figure 15 shows SEM image of specimen 2 with three different surface topographies: non-melted particles stuck to the surface (green arrows), particles due to balling phenomena (yellow particles), and bump structures (blue arrows). During laser scanning of the powder bed, some powder particles may not be fully melted, and these non-fully melted particles can attach to the surface and increase the surface roughness of the specimen [45]. On the surface of the specimens, some spherical or ellipsoidal particles can be observed due to balling phenomenon. During laser scanning, liquified powders in melt pool tend to wet the neighborhood non-melted powders. However, due to the surface tension effect, the wetting ability of molten liquid decreases causing splashed particles out from the melt pool

[46–48]. These particles due to balling phenomenon can also increase surface roughness of the specimens. Apart from these, due to the increase in the viscosity of molten metal in melt pool, melt pool expansion occurs which result in bumps or mushroom-like structures on the surface. This phenomenon can also increase the surface roughness. Figure 15 also reveals some microcracks present on the surface (red arrows). It was stated in the literature that these microcracks initiate severe cracks and decrease the fatigue life of the specimens [49].

3.3 Microhardness results

Three microhardness measurements were performed through the thickness of the part, near to the upper face, at the middle, near to the downskin face, and average of them which are shown in Figs. 16, 17 and 18 in terms of support

Fig. 17 The effect of support thickness and spacing on microhardness for 0.31 mm support gap

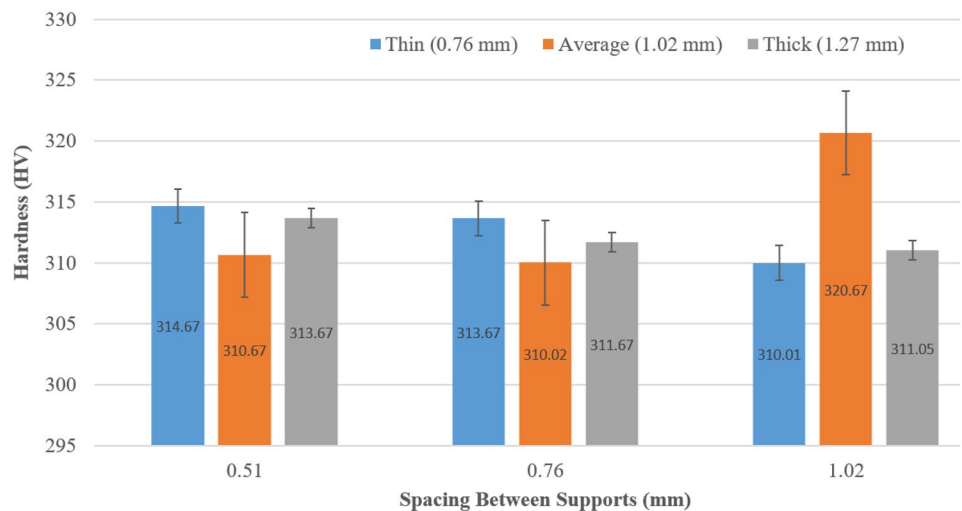
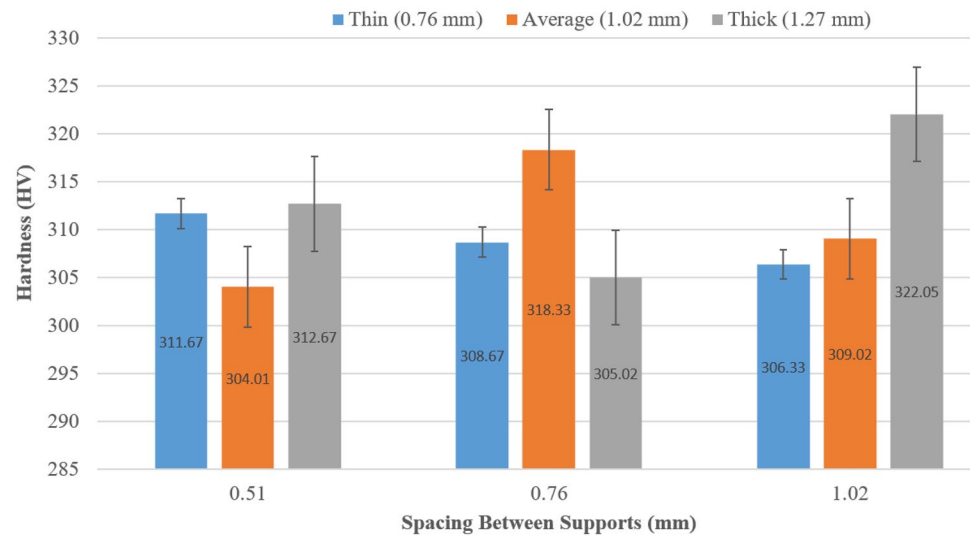


Fig. 18 The effect of support thickness and spacing on microhardness for 0.38 mm support gap



thickness and support spacing. The minimum average microhardness (304 HV) was observed at 0.38 mm support gap, 0.51 mm support spacing, and 1.02 mm support thickness. On the other hand, the maximum average microhardness

(322 HV) was observed at 0.38 mm support gap, 1.02 mm support spacing, and 1.27 mm support thickness. The microhardness measurement results are consistent with the results in literature [50].

Microstructure of upskin surface, mid-surface, and downskin surface along with microhardness measurements is shown in Fig. 19. It is obvious that microhardness at downskin surface is higher than the microhardness at the mid- and upskin surfaces. The increase of microhardness at the downskin surface of the specimens can be attributed to the formation of finer microstructure at the downskin surface than the upskin surface where coarser microstructure was observed as shown in Fig. 19. Grain size increase from downskin surface to the upfacing surface as shown in Fig. 19 can be attributed to the thermal cycle change during printing. At downskin area, due to the large thermal gradient between surface and the contactless support, high cooling rate based on conduction and fine grains can be obtained [51]. When build height increases towards the upfacing surface, conduction and convection phenomena towards the surrounding powders become more dominant resulting in coarser grains [52]. Figure 20 shows cross-sectional optical microscope image of specimen 14. It is clear that some particles were fused to the overhang surface. After melt pool penetration to the powder bed during laser scanning, some non-fully melted powders can fuse to the overhang surface during solidification. These fused powders change the thermal behavior of interface surface and microstructure. Columnar grain structures starting from the interface between fused particle and the material and protruding to the inside of the material can change the hardness behavior of the specimens [53]. In Fig. 20, some inner porosities can also be observed. These porosities decrease the mechanical behavior of the specimen.

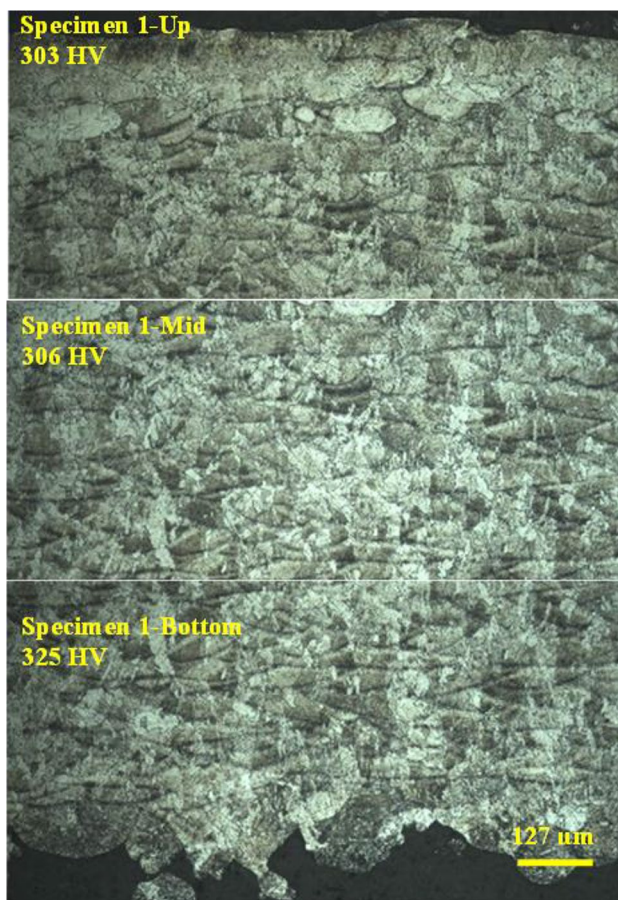


Fig. 19 Microhardness through thickness of specimen 1

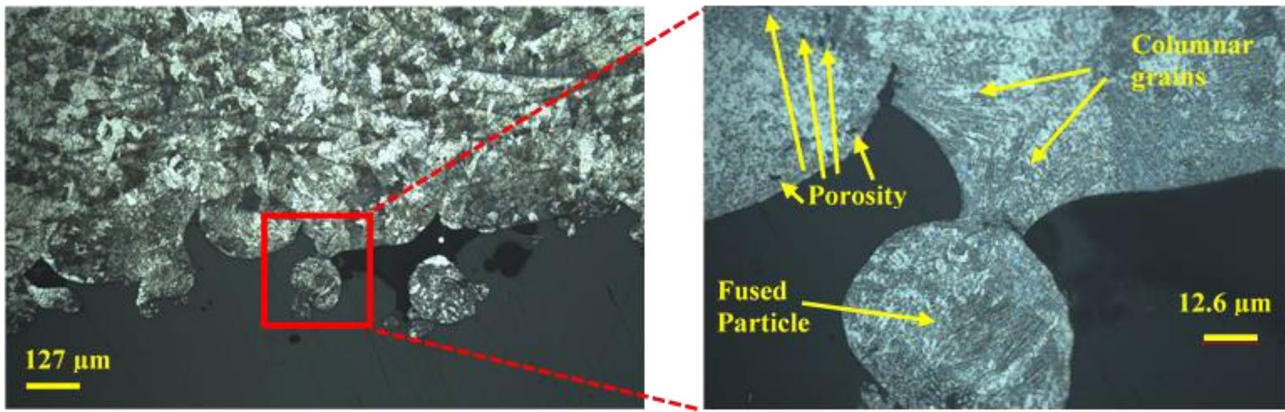


Fig. 20 Cross-sectional optical microscope image of specimen 14

4 Conclusion

This experimental study investigated the effect of contactless support gap, segmented contactless support thickness, and spacing between each segment on dimensional deviation, surface roughness, microhardness through thickness, and microstructure of the overhang thin wall specimens produced by LPBF process from Inconel 718 material. The following main conclusions can be drawn:

- High-dimensional deviation is one of the drawbacks of LPBF process. In the present study, it was observed that decreasing support thickness, support spacing, or support gap increases the dimensional accuracy.
- Thickness deviation is more susceptible to changes in support spacing for thinner support than thicker ones.
- Complicated and higher deviations were observed on downskin surfaces than upfacing surfaces. Moreover, due to free edge effect, tip of the thin wall specimens showed higher deviations than the root of the specimens.
- It was observed that surface roughness can be decreased by decreasing spacing between each support segments.
- Sticking of non-fully melted particles to the overhang surfaces, particles due to balling effect and bump structures were observed on downskin surfaces for nearly all specimens. These surface irregularities are the main causes of high-dimensional variations and surface roughness values.
- Microstructure through the thickness changes from coarse microstructure at near up face to fine microstructure at near bottom face. Due to this microstructure change, microhardness was observed to be higher at downskin surfaces than upfacing surfaces.
- Columnar grain formation at the interface between fused particles and the overhang surface was observed in nearly all specimens which also increases the microhardness at overhang surface.

Author contribution The study conception and design were performed by Orhan Gülcan. Material preparation and data collection and analysis were performed by Orhan Gülcan, Kadir Günaydın, and Alican Çelik. Discussion was performed by Orhan Gülcan, Kadir Günaydın, and Evren Yasa. The first draft of the manuscript was written by Orhan Gülcan, and all authors commented on previous versions of the manuscript. All authors read and approved the final manuscript.

Funding This study was carried out under the Scientific and Technological Council of Turkey (TUBITAK) Technology and Innovation Support Program (Grant number: 5158001).

Declarations

Competing interests The authors declare no competing interests.

References

1. Flores I, Kretschmar N, Azman AH, Chekurov S, Pedersen DB, Chaudhuri A (2020) Implications of lattice structures on economics and productivity of metal powder bed fusion. *Addit Manuf* 31:100947. <https://doi.org/10.1016/j.addma.2019.100947>
2. Leary M (2020) Powder bed fusion. In: Martin L (ed) *Additive manufacturing materials and technologies, design for additive manufacturing*, Elsevier, Netherlands, pp. 295–319. <https://doi.org/10.1016/B978-0-12-816721-2.00011-7>
3. Kuo YH, Cheng CC (2019) Self-supporting structure design for additive manufacturing by using a logistic aggregate function. *Struct Multidiscipl Optim* 60:1109–1121. <https://doi.org/10.1007/s00158-019-02261-3>
4. Leary M, Maconachie T, Sarker A, Faruque O, Brandt M (2019) Mechanical and thermal characterisation of AlSi10Mg SLM block support structures. *Mater Des* 183:108138. <https://doi.org/10.1016/j.matdes.2019.108138>
5. Jiang J, Xu X, Stringer J (2018) Support structures for additive manufacturing: a review. *J Manuf Mater Process* 2:64. <https://doi.org/10.3390/jmmp2040064>
6. Järvinen JP, Matilainen V, Li X, Piili H, Salminen A, Mäkelä I, Nyrhilä O (2014) Characterization of effect of support structures in laser additive manufacturing of stainless steel. *Phys Procedia* 56:72–81. <https://doi.org/10.1016/j.phpro.2014.08.099>
7. Cao Q, Bai Y, Zhang J, Shi Z, Fuh JYH, Wang H (2020) Removability of 316L stainless steel cone and block support

- structures fabricated by selective laser melting (SLM). *Mater Des* 191:108691. <https://doi.org/10.1016/j.matdes.2020.108691>
8. Ameen W, Al-Ahmari A, Mohammed MK (2019) Self-supporting overhang structures produced by additive manufacturing through electron beam melting. *Int J Adv Manuf Technol* 104:2215–2232. <https://doi.org/10.1007/s00170-019-04007-3>
 9. Huang R, Dai N, Cheng X, Wang L (2020) Topology optimization of lattice support structures for heat conduction in selective laser melting. *Int J Adv Manuf Technol* 109:1841–1851. <https://doi.org/10.1007/s00170-020-05741-9>
 10. Zeng K (2015) Optimization of support structures for selective laser melting. Dissertation, University of Louisville
 11. Gan MX, Wong CH (2016) Practical support structures for selective laser melting. *J Mater Process Technol* 238:474–484. <https://doi.org/10.1016/j.jmatprotec.2016.08.006>
 12. Lindecke PNJ, Blunk H, Wenzl JP, Möller M, Emmelmann C (2018) Optimization of support structures for the laser additive manufacturing of TiAl6V4 parts. *Procedia CIRP* 74:53–58. <https://doi.org/10.1016/j.procir.2018.08.029>
 13. Calignano F (2014) Design optimization of supports for overhanging structures in aluminum and titanium alloys by selective laser melting. *Mater Des* 64:203–213. <https://doi.org/10.1016/j.matdes.2014.07.043>
 14. Poyraz Ö, Yasa E, Akbulut G, Orhangül A, Pilatin S (2015) Investigation of support structures for direct metal laser sintering (DMLS) of In625 Parts. *Solid Freeform Fabrication Symposium, Austin, Texas, USA*, pp. 560–574
 15. Umer U, Ameen W, Abidi MH, Moiduddin K, Alkhalefah H, Alkahtani M, Al-Ahmari A (2019) Modeling the effect of different support structures in electron beam melting of titanium alloy using finite element models. *Metals* 9:806. <https://doi.org/10.3390/met9070806>
 16. Ameen W, Mohammed MK, Al-Ahmari A (2019) Evaluation of support structure removability for additively manufactured Ti6Al4V overhangs via electron beam melting. *Metals* 9:1211. <https://doi.org/10.3390/met9111211>
 17. Hussein A, Hao L, Yan C, Everson R, Young P (2013) Advanced lattice support structures for metal additive manufacturing. *J Mater Process Technol* 213:1019–1026. <https://doi.org/10.1016/j.jmatprotec.2013.01.020>
 18. Strano G, Hao L, Everson RM, Evans KE (2013) A new approach to the design and optimization of support structures in additive manufacturing. *Int J Adv Manuf Technol* 66:1247–1254. <https://doi.org/10.1007/s00170-012-4403-x>
 19. Das P, Chandran R, Samant R, Anand S (2015) Optimum part build orientation in additive manufacturing for minimizing part errors and support structures. *Procedia Manuf* 1:343–354. <https://doi.org/10.1016/j.promfg.2015.09.041>
 20. Zhang X, Kang J, Rong Y, Wu P, Feng T (2019) Effect of scanning routes on the stress and deformation of overhang structures fabricated by SLM. *Materials* 12:47. <https://doi.org/10.3390/ma12010047>
 21. Allaire G, Bogosel B (2018) Optimizing supports for additive manufacturing. *Struct Multidiscipl Optim* 58:2493–2515. <https://doi.org/10.1007/s00158-018-2125-x>
 22. Das P, Mhapsekar K, Chowdhury S, Samant R, Anand S (2017) Selection of build orientation for optimal support structures and minimum part errors in additive manufacturing. *Comput Aided Des Appl* 14(1):1–13. <https://doi.org/10.1080/16864360.2017.1308074>
 23. Pellens J, Lombaert G, Michiels M, Craeghs T, Schevenels M (2020) Topology optimization of support structure layout in metal-based additive manufacturing accounting for thermal deformations. *Struct Multidiscipl Optim* 61:2291–2303. <https://doi.org/10.1007/s00158-020-02512-8>
 24. Allaire G, Bihr M, Bogosel B (2020) Support optimization in additive manufacturing for geometric and thermo-mechanical constraints. *Struct Multidiscipl Optim* 61:2377–2399. <https://doi.org/10.1007/s00158-020-02551-1>
 25. Zhou M, Liu Y, Wei C (2020) Topology optimization of easy-removal support structures for additive manufacturing. *Struct Multidiscipl Optim* 61:2423–2435. <https://doi.org/10.1007/s00158-020-02607-2>
 26. Zhang Y, Wang Z, Zhang Y, Gomes S, Bernard A (2020) Bio-inspired generative design for support structure generation and optimization in additive manufacturing (AM). *CIRP Ann Manuf Technol* 69(1):117–120. <https://doi.org/10.1016/j.cirp.2020.04.091>
 27. Zhou M, Liu Y, Lin Z (2019) Topology optimization of thermal conductive support structures for laser additive manufacturing. *Comput Methods Appl Mech Eng* 353:24–43. <https://doi.org/10.1016/j.cma.2019.03.054>
 28. McConaha M, Venugopal V, Anand S (2020) Integration of machine tool accessibility of support structures with topology optimization for additive manufacturing. *Procedia Manuf* 48:634–642. <https://doi.org/10.1016/j.promfg.2020.05.092>
 29. Mirzendehtdel AM, Behandish M, Nelaturi S (2021) Topology optimization for manufacturing with accessible support structures. <https://arxiv.org/abs/2108.02829>. Accessed 10 June 2022
 30. Morgan D, Agba E, Hill C (2017) Support structure development and initial results for metal powder bed fusion additive manufacturing. *Procedia Manuf* 10:819–830. <https://doi.org/10.1016/j.promfg.2017.07.083>
 31. Chou Y-S, Cooper K (2015) Systems and methods for designing and fabricating contact-free support structures for overhang geometries of parts in powder-bed metal additive manufacturing. <https://patents.google.com/patent/US20170136539A1/en>. Accessed 10 June 2022
 32. Wang X, Chou K (2018) Effect of support structures on Ti-6Al-4V overhang parts fabricated by powder bed fusion electron beam additive manufacturing. *J Mater Process Technol* 257:65–78. <https://doi.org/10.1016/j.jmatprotec.2018.02.038>
 33. Cheng B, Chou K (2015) Geometric consideration of support structures in part overhang fabrications by electron beam additive manufacturing. *Comput Aided Des* 69:102–111. <https://doi.org/10.1016/j.cad.2015.06.007>
 34. Cooper K, Steele P, Cheng B, Chou K (2018) Contact-free support structures for part overhangs in powder-bed metal additive manufacturing. *Inventions* 3(1):2. <https://doi.org/10.3390/inventions3010002>
 35. Zhang K, Fu G, Zhang P, Ma Z, Mao Z, Zhang DZ (2019) Study on the geometric design of supports for overhanging structures fabricated by selective laser melting. *Materials* 12:27. <https://doi.org/10.3390/ma12010027>
 36. Cheng B, Chou YK (2017) Overhang support structure design for electron beam additive manufacturing. *Proceedings of the ASME 2017 12th International Manufacturing Science and Engineering Conference*, June 4–8, Los Angeles, CA, USA
 37. Cheng B, Chou K (2020) A numerical investigation of support structure designs for overhangs in powder bed electron beam additive manufacturing. *J Manuf Process* 49:187–195. <https://doi.org/10.1016/j.jmappro.2019.11.018>
 38. Kurzynowski T, Stopyra W, Gruber K, Ziółkowski G, Kuźnicka B, Chlebus E (2019) Effect of scanning and support strategies on relative density of SLM-ed H13 steel in relation to specimen size. *Materials* 12:239. <https://doi.org/10.3390/ma12020239>
 39. Kouraytem N, Chanut RA, Watring DS, Loveless T, Varga J, Spear AD, Kingstedt OT (2020) Dynamic-loading behavior and anisotropic deformation of pre- and post-heat-treated In718 fabricated by laser powder bed fusion. *Addit Manuf* 33:101083. <https://doi.org/10.1016/j.addma.2020.101083>

40. Sing SL, Miao Y, Wiria FE, Yeong WY (2016) Manufacturability and mechanical testing considerations of metallic scaffolds fabricated using selective laser melting: a review. *Biomed Sci Eng* 2(11):18–24. <https://doi.org/10.4081/bse.2016.11>
41. Bartolomeu F, Fonseca J, Peixinho N, Alves N, Gasik M, Silva FS, Miranda G (2019) Predicting the output dimensions, porosity and elastic modulus of additive manufactured biomaterial structures targeting orthopedic implants. *J Mech Behav Biomed Mater* 99:104–117. <https://doi.org/10.1016/j.jmbbm.2019.07.023>
42. Bartolomeu F, Dourado N, Pereira F, Alves N, Miranda G, Silva FS (2020) Additive manufactured porous biomaterials targeting orthopedic implants: a suitable combination of mechanical, physical and topological properties. *Mater Sci Eng C* 107:110342. <https://doi.org/10.1016/j.msec.2019.110342>
43. Ran Q, Yang W, Hu Y, Shen X, Yu Y, Xiang Y, Cai K (2018) Osteogenesis of 3D printed porous Ti6Al4V implants with different pore sizes. *J Mech Behav Biomed Mater* 84:1–11. <https://doi.org/10.1016/j.jmbbm.2018.04.010>
44. Newton L, Senin N, Gomez C, Danzl R, Helml F, Blunt L, Leach R (2019) Areal topography measurement of metal additive surfaces using focus variation microscopy. *Addit Manuf* 25:365–389. <https://doi.org/10.1016/j.addma.2018.11.013>
45. Xiao Z, Yang Y, Xiao R, Bai Y, Song C, Wang D (2018) Evaluation of topology optimized lattice structures manufactured via selective laser melting. *Mater Des* 143:27–37. <https://doi.org/10.1016/j.matdes.2018.01.023>
46. Li R, Liu J, Shi Y, Wang L, Jiang W (2012) Balling behavior of stainless steel and nickel powder during selective laser melting process. *Int J Adv Manuf Technol* 59:1025–1035. <https://doi.org/10.1007/s00170-011-3566-1>
47. Boutaous M, Liu X, Siginer DA, Xin S (2021) Balling phenomenon in metallic laser based 3D printing process. *Int J Therm Sci* 167:107011. <https://doi.org/10.1016/j.ijthermalsci.2021.107011>
48. Dwivedi S, Dixit AR, Das AK (2022) Wetting behavior of selective laser melted (SLM) bio-medical grade stainless steel 316L. *Mater Today: Proc* 56(1):46–50. <https://doi.org/10.1016/j.matpr.2021.12.046>
49. Ren D, Li S, Wang H, Hou W, Hao Y, Jin W, Yang R, Devesh R, Misra K, Murr LE (2019) Fatigue behavior of Ti-6Al-4V cellular structures fabricated by additive manufacturing technique. *J Mater Sci Technol* 35:285–294. <https://doi.org/10.1016/j.jmst.2018.09.066>
50. Karabulut Y, Tascioglu E, Kaynak Y (2021) Heat treatment temperature-induced microstructure, microhardness and wear resistance of Inconel 718 produced by selective laser melting additive manufacturing. *Optik* 227:163907. <https://doi.org/10.1016/j.ijleo.2019.163907>
51. Seede R, Mostafa A, Brailovski V, Jahazi M, Medraj M (2018) Microstructural and microhardness evolution from homogenization and hot isostatic pressing on selective laser melted Inconel 718: structure, texture, and phases. *J Manuf Mater Process* 2(2):30. <https://doi.org/10.3390/jmmp2020030>
52. Zhang B, Wang P, Chew Y, Wen Y, Zhang M, Wang P, Bi G, Wei J (2020) Mechanical properties and microstructure evolution of selective laser melting Inconel 718 along building direction and sectional dimension. *Mater Sci Eng: A* 794:139941. <https://doi.org/10.1016/j.msea.2020.139941>
53. Qi M, Huang S, Ma Y, Youssef SS, Zhang R, Qiu J, Lei J, Yang R (2021) Columnar to equiaxed transition during β heat treatment in a near β alloy by laser additive manufacture. *J Mater Res Technol* 13:1159–1168. <https://doi.org/10.1016/j.jmrt.2021.05.057>

Publisher's Note Springer Nature remains neutral with regard to jurisdictional claims in published maps and institutional affiliations.

Springer Nature or its licensor holds exclusive rights to this article under a publishing agreement with the author(s) or other rightsholder(s); author self-archiving of the accepted manuscript version of this article is solely governed by the terms of such publishing agreement and applicable law.